Maximum-Diversity Transmissions Over Doubly Selective Wireless Channels

Xiaoli Ma, *Student Member, IEEE,* and
Georgios B. Giannakis, *Fellow, IEEE*

***Abstract*—High data rates and multipath propagation give rise to frequency-selectivity of wireless channels, while carrier frequency offsets and mobility-induced Doppler shifts introduce time-selectivity in wireless links. The resulting time- and frequency-selective (or doubly selective) channels offer joint multipath–Doppler diversity gains. Relying on a basis expansion model of the doubly selective channel, we prove that the maximum achievable multipath–Doppler diversity order is determined by the rank of the correlation matrix of the channel's expansion coefficients, and is multiplicative in the effective degrees of freedom that the channel exhibits in the time and frequency dimensions. Interestingly, it turns out that time–frequency reception alone does not guarantee maximum diversity, unless the transmission is also designed judiciously. We design such block precoded transmissions. The corresponding designs for frequency-selective or time-selective channels follow as special cases, and thorough simulations are provided to corroborate our theoretical findings.**

***Index Terms*—Diversity, Doppler, doubly selective channels, fading, multipath, precoding, time-selective channels.**

I. Introduction

Wireless channels with delay spread exceeding the symbol period introduce frequency-selectivity which increases along with the demand for higher data rates. Furthermore, temporal channel variations arising due to relative mobility between transmitter and receiver, as well as due to oscillator drifts and phase noise, give rise to time-selectivity. The combined time–frequency-selectivity induces delay-Doppler fading, which affects critically communication performance. Therefore, modeling channel variations, and devising countermeasures against time- and frequency-selective fading are important and challenging tasks in the design of wireless and mobile communication systems.

Diversity techniques are known to offer valuable countermeasures against fading [9]. Frequency-selective channels offer *multipath diversity* [15], while time-selective channels can provide *Doppler diversity* [12]. Based on a basis expansion model (BEM), we adopt for time-selective frequency-flat channels [1], [13], [4], [12], [2], we will show that the maximum Doppler diversity order equals the number of bases $(Q+1)$. Subsequently, we will design linearly precoded transmissions capable of enabling this maximum diversity order. Linearly precoded transmissions over frequency-selective channels of order L were designed in [15] to enable the maximum possible multipath diversity of order $L+1$. Capitalizing on the time-selective results here along with those of [15] for frequency-selective channels, we will then focus on doubly selective channels that entail more degrees of freedom. With *uncorrelated* taps, doubly selective channels offer the potential for even higher (two-dimensional) diversity order $(L+1)(Q+1)$, that is, multiplicative in the multipath-Doppler dimensions [12]. We will also design linearly precoded transmissions that guarantee this maximum diversity, when maximum-likelihood (ML) decoding is employed. The rank of the channel correlation matrix will determine the maximum diversity order for *correlated* channels.

Time–frequency RAKE receivers have been developed for collecting diversity gains in a spread-spectrum (SS) setup [12], [2]. However, the resulting time–frequency RAKE receivers can only benefit from receive diversity, and do not enable the joint multipath-Doppler diversity provided by the channel. In addition to allowing for non-SS point-to-point links, our contributions relative to [2], [12] include the analytical formulation of the maximum achievable diversity order for doubly selective (and possibly correlated) channels, and the transmitter design. As a by-product, the single-user results here show that the multiple-access schemes of [7] collect the maximum available diversity.

The organization of the correspondence is as follows. Section II briefly introduces our time-varying (TV) channel model. Section III deals with maximum diversity transmissions. Time-selective-only channels are discussed first, followed by the time- and frequency-selective ones. Several transmitter designs are derived to enable the maximum diversity order. The bandwidth efficiency of these designs is also provided. Section IV verifies the appropriateness of the BEM, and confirms our diversity claims, by simulations. Section V concludes this correspondence.

Notation: Upper (lower) bold face letters will be used for matrices (column vectors). Superscript $\mathcal{H}$ will denote Hermitian, $*$ conjugate, and T transpose. We will reserve $\otimes$ for Kronecker product, $\lceil\cdot\rceil$ for integer ceiling, $\lfloor\cdot\rfloor$ for integer floor, and $E[\cdot]$ for expectation with respect to all the random variables within the brackets. We will use $[\boldsymbol{A}]_{k,\,m}$ to denote the $(k,\,m)$th entry of a matrix $\boldsymbol{A}$, and $[\boldsymbol{x}]_m$ to denote the mth entry of the column vector $\boldsymbol{x}$; $\boldsymbol{I}_N$ will denote the $N\times N$ identity matrix; $[\boldsymbol{F}_N]_{k,\,m}:=N^{-1/2}\exp(-j2\pi km/N)$, the $N\times N$ fast Fourier transform (FFT) matrix; finally, $\mathrm{diag}\,[\boldsymbol{x}]$ will stand for a diagonal matrix with $\boldsymbol{x}$ on its main diagonal.

II. Time- and Frequency-Selective Channel Model

Let $c(t;\,\tau)$ denote the continuous-time baseband equivalent channel impulse response of the TV channel given by the convolution of the transmit filter, the receive filter, and the TV physical channel. With $C(f;\,\tau)$ denoting the Fourier transform of $c(t;\,\tau)$, let us also define the delay spread, $\tau_{\max}$, and the Doppler spread, $f_{\max}$, as the thresholds for which: $|C(f;\,\tau)|\approx 0$, for $|\tau|>\tau_{\max}$, or $|f|>f_{\max}$. We will take the sampling period at the receiver equal to the symbol period T_s, and we will consider time intervals of NT_s seconds corresponding to blocks containing N symbols each. Because the channel is approximately band limited, for each block interval, say the nth with $t\in[nNT_s,\,(n+1)NT_s)$, the channel variation can be represented by: a) finite coefficients that remain invariant per block, but are allowed to change with n; and b) finite Fourier bases that capture the time variation, but are common $\forall\, n$. Using the serial index i, we can describe the block index as $n:=\lfloor i/N\rfloor$, and write our *discrete-time baseband equivalent* channel model as

$$h(i;\,l)=\sum_{q=0}^{Q}h_q(n;\,l)e^{j\omega_q i},\qquad l\in[0,\,L] \tag{1}$$

where $\omega_q:=2\pi(q-Q/2)/N$, $L:=\lceil\tau_{\max}/T_s\rceil$, and $Q:=2\lceil f_{\max}NT_s\rceil$. We will refer to our channel model in (1) as the BEM. Because both $\tau_{\max}$ and $f_{\max}$ can be measured experimentally in practice, we assume the following.

A1) *Parameters* $\tau_{\max}$, $f_{\max}$ (*and, thus,* L, Q) *are bounded, known, and satisfy*: $2f_{\max}\tau_{\max}<1$.

Manuscript received September 7, 2001; revised September 22, 2002. This work was supported by the ARL/CTA under Grant DAAD19-01-2-011. The material in this correspondence was presented in part at the 39th Annual Allerton Conference on Communication, Control, and Computing, Monticello, IL, October 2001 and the IEEE Wireless Communications and Networking Conference, Orlando, FL, March 2002.

The authors are with the Department of Electrical and Computer Engineering, University of Minnesota, Minneapolis, MN 55455 USA (e-mail: xiaoli@ece.umn.edu; georgios@ece.umn.edu).

Communicated by G. Caire, Associate Editor for Communications.
Digital Object Identifier 10.1109/TIT.2003.813485

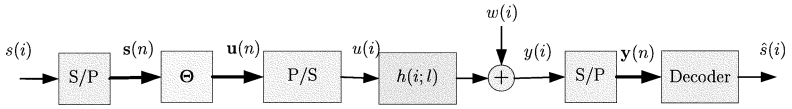

Fig. 1. Discrete-time baseband equivalent model.

The product $2f_{\max}\tau_{\max}$ is called the delay-Doppler spread factor, and plays an important role in estimating doubly selective channels. Underspread systems satisfy $2f_{\max}\tau_{\max} < 1$, which, intuitively speaking, bounds the channel's degrees of freedom and renders channel estimation well posed [6]. In fact, most ionospheric and tropospheric scattering as well as other radio channels all give rise to underspread channels; see, e.g., [9, p. 816].

When transmissions experience rich scattering, and no line-of-sight is present, one can appeal to the central limit theorem to validate the following assumption.

A2) *The BEM coefficients $h_q(n;\, l)$ are zero-mean, complex Gaussian random variables.*

We note that related sampled representations of time- and frequency-selective channels have also been advocated in [1], [13], [4], [12], [2].

III. Block Transmissions and Diversity

Fig. 1 depicts the discrete-time equivalent transmission model when communicating through the doubly selective channel (1), where P/S and S/P denote parallel-to-serial and serial-to-parallel operations, respectively. The information stream $s(i)$ is drawn from a finite alphabet, and parsed into blocks of size N_s. We use two arguments (n and k) to describe the serial index $i = nN_s + k$ for $k \in [0,\, N_s - 1]$ and denote the $(k+1)$th entry of the nth block as $[\boldsymbol{s}(n)]_k := s(nN_s + k)$. Each block $\boldsymbol{s}(n)$ is linearly precoded by an $N \times N_s$ matrix $\boldsymbol{\Theta}$ to yield $N \times 1$ symbol blocks $\boldsymbol{u}(n) = \boldsymbol{\Theta}\boldsymbol{s}(n)$, where $N \geq N_s$. The matrix $\boldsymbol{\Theta}$ will play an instrumental role in designing maximum diversity transmissions.

After P/S multiplexing, the blocks $\boldsymbol{u}(n)$ are transmitted through the time- and frequency-selective channel $h(i;\, l)$. The ith received sample $y(i)$ can be written as

$$y(i) = \sum_{l=0}^{L} h(i;\, l)u(i-l) + w(i) \tag{2}$$

where $w(i)$ is additive white Gaussian noise (AWGN) with mean zero, and variance $N_0/2$.

In the remainder of this section, we will define and quantify the diversity order. We will also design the precoder $\boldsymbol{\Theta}$ to ensure maximum diversity transmissions through (possibly correlated) doubly selective channels. We will find it convenient to work with a block form of the BEM which we construct, after S/P conversion, by collecting the samples $y(i)$ into $N \times 1$ blocks: $[\boldsymbol{y}(n)]_k = y(nN + k)$, $k \in [0,\, N-1]$. Selecting also $N \geq L$, we can write the matrix–vector counterpart of (2) as

$$\boldsymbol{y}(n) = \boldsymbol{H}^{(0)}(n)\boldsymbol{\Theta}\boldsymbol{s}(n) + \boldsymbol{H}^{(1)}(n)\boldsymbol{\Theta}\boldsymbol{s}(n-1) + \boldsymbol{w}(n) \tag{3}$$

where $[\boldsymbol{w}(n)]_k := w(nN + k)$, $k \in [0,\, N-1]$, and $\boldsymbol{H}^{(0)}(n)$ and $\boldsymbol{H}^{(1)}(n)$ are $N \times N$ lower and upper triangular matrices with entries

$$[\boldsymbol{H}^{(r)}(n)]_{k,\,m} = h(nN + k;\, rN + k - m)$$

for $r = 0,\, 1$, and $k,\, m \in [0,\, N-1]$. The second term in the right-hand side (RHS) of (3) captures the interblock interference (IBI) that emerges due to the channel delay spread. Recalling that $i = nN + k$ in (1), we can rewrite these channel matrices as

$$\boldsymbol{H}^{(r)}(n) = \sum_{q=0}^{Q} \boldsymbol{D}(\omega_q)\boldsymbol{H}_q^{(r)}(n), \qquad r = 0,\, 1 \tag{4}$$

where

$$\boldsymbol{D}(\omega_q) := \mathrm{diag}[1,\, \ldots,\, \exp(j\omega_q(N-1))]$$

$\boldsymbol{H}_q^{(0)}(n)$ and $\boldsymbol{H}_q^{(1)}(n)$ are lower and upper triangular Toeplitz matrices with entries $[\boldsymbol{H}_q^{(r)}(n)]_{k,\,m} = h_q(n;\, rN + k - m)$. According to the BEM in (1), the bases that vary within each block are described by the diagonal matrices $\{\boldsymbol{D}(\omega_q)\}_{q=0}^{Q}$ in (4), separately from the time-invariant channel coefficients that are collected in matrices $\{\boldsymbol{H}_q^{(r)}(n)\}_{q=0}^{Q}$. Based on (4), the diversity-maximizing transmissions over TV channels will obtain similar forms to those for time-invariant channels.

A. Time-Selective Frequency-Flat-Fading Channels

A time-selective frequency-flat-fading channel is a special case of a doubly selective channel corresponding to order $L = 0$. Only in this subsection, we will drop the channel tap index l and without loss of generality, we will also drop the block index n. Since the channel considered here is time selective only, it has no memory, and thus the IBI is absent. In this case, (4) reduces to $\boldsymbol{H}^{(0)} := \sum_{q=0}^{Q} h_q\boldsymbol{D}(\omega_q)$, and (3) can be rewritten as

$$\boldsymbol{y} = \sum_{q=0}^{Q} h_q\boldsymbol{D}(\omega_q)\boldsymbol{\Theta}\boldsymbol{s} + \boldsymbol{w} = \boldsymbol{\Phi}_s\boldsymbol{h} + \boldsymbol{w} \tag{5}$$

where the channel vector $\boldsymbol{h}$ and the matrix $\boldsymbol{\Phi}_s$ are defined, respectively, as

$$\boldsymbol{h} := [h_0 \cdots h_Q]^T$$

and

$$\boldsymbol{\Phi}_s := [\boldsymbol{D}(\omega_0)\boldsymbol{\Theta}\boldsymbol{s} \cdots \boldsymbol{D}(\omega_Q)\boldsymbol{\Theta}\boldsymbol{s}]. \tag{6}$$

We will resort to a pair-wise error probability (PEP) technique to examine the maximum achievable diversity order of BEM-based time-selective channels.

Assuming that perfect channel status information (CSI) is available at the receiver, and that ML decoding is employed, we consider the PEP, $P(\boldsymbol{s} \to \boldsymbol{s}'|\boldsymbol{h})$, that a block $\boldsymbol{s}$ is transmitted but is incorrectly decoded as $\boldsymbol{s}' \neq \boldsymbol{s}$. The PEP can be approximated using the Chernoff bound [9, p. 53] as

$$P(\boldsymbol{s} \to \boldsymbol{s}'|\boldsymbol{h}) \leq \exp(-d^2(\boldsymbol{x},\, \boldsymbol{x}')/4N_0)$$

where $\boldsymbol{x} := \boldsymbol{H}^{(0)}\boldsymbol{\Theta}\boldsymbol{s}$, $\boldsymbol{x}' := \boldsymbol{H}^{(0)}\boldsymbol{\Theta}\boldsymbol{s}'$,

$$d^2(\boldsymbol{x},\, \boldsymbol{x}') := \|\boldsymbol{x} - \boldsymbol{x}'\|^2 = (\boldsymbol{x} - \boldsymbol{x}')^{\mathcal{H}}(\boldsymbol{x} - \boldsymbol{x}')$$

is the Euclidean distance between $\boldsymbol{x}$ and $\boldsymbol{x}'$, and $N_0/2$ is the AWGN variance.

With $\boldsymbol{e} := \boldsymbol{s} - \boldsymbol{s}'$ denoting the error vector, we express the distance between $\boldsymbol{x}$ and $\boldsymbol{x}'$ as $d^2(\boldsymbol{x},\, \boldsymbol{x}') = \|\boldsymbol{H}^{(0)}\boldsymbol{\Theta}\boldsymbol{e}\|^2 = \|\boldsymbol{\Phi}_e\boldsymbol{h}\|^2$, where $\boldsymbol{\Phi}_e$ is defined as $\boldsymbol{\Phi}_s$ with $\boldsymbol{e}$ replacing $\boldsymbol{s}$ in (6). Because our analysis will allow for correlated channels, we will denote the $(Q+1) \times (Q+1)$ channel autocorrelation matrix and its rank, respectively, by

$$\boldsymbol{R}_h := E[\boldsymbol{h}\boldsymbol{h}^{\mathcal{H}}] \quad \text{and} \quad r_h := \mathrm{rank}(\boldsymbol{R}_h) \leq Q + 1. \tag{7}$$

Eigenvalue decomposition of $\boldsymbol{R}_h$ yields $\boldsymbol{R}_h = \boldsymbol{V}_h\boldsymbol{D}_h\boldsymbol{V}_h^{\mathcal{H}}$, where

$$\boldsymbol{D}_h := \mathrm{diag}[\sigma_0^2,\, \sigma_1^2,\, \ldots,\, \sigma_{r_h-1}^2]$$

and $\boldsymbol{V}_h$ is a $(Q+1) \times r_h$ matrix satisfying $\boldsymbol{V}_h^{\mathcal{H}}\boldsymbol{V}_h = \boldsymbol{I}_{r_h}$. Define an $r_h \times 1$ normalized channel vector $\overline{\boldsymbol{h}}$ whose entries are independent and identically distributed (i.i.d.) Gaussian random variables with zero

mean and unit variance. It is not difficult to show that $\boldsymbol{h}$ and $\boldsymbol{V}_h\boldsymbol{D}_h^{\frac{1}{2}}\overline{\boldsymbol{h}}$ have identical distributions. Therefore, the PEP remains statistically invariant when one replaces $\boldsymbol{h}$ by $\boldsymbol{V}_h\boldsymbol{D}_h^{\frac{1}{2}}\overline{\boldsymbol{h}}$. To proceed, let us define the matrix

$$\boldsymbol{A}_e := (\boldsymbol{V}_h\boldsymbol{D}_h^{\frac{1}{2}})^{\mathcal{H}}\boldsymbol{\Phi}_e^{\mathcal{H}}\boldsymbol{\Phi}_e\boldsymbol{V}_h\boldsymbol{D}_h^{\frac{1}{2}}.$$

Since $\boldsymbol{A}_e$ is Hermitian, there exists a unitary matrix $\boldsymbol{V}_e$ and a real nonnegative definite diagonal matrix $\boldsymbol{D}_e$, so that $\boldsymbol{V}_e^{\mathcal{H}}\boldsymbol{A}_e\boldsymbol{V}_e = \boldsymbol{D}_e$. The $r_h\times r_h$ diagonal matrix $\boldsymbol{D}_e := \mathrm{diag}[\lambda_0, \ldots, \lambda_{r_h-1}]$ holds on its diagonal the eigenvalues of $\boldsymbol{A}_e$, that satisfy $\lambda_q \geq 0, \forall\, q \in [0,\, r_h-1]$. The vector $\tilde{\boldsymbol{h}} = \boldsymbol{V}_e\overline{\boldsymbol{h}}$ has correlation identical to $\overline{\boldsymbol{h}}$ because $\boldsymbol{V}_e$ is unitary. If $r_a(e) := \mathrm{rank}(\boldsymbol{A}_e)$, then $r_a(e)$ eigenvalues of $\boldsymbol{A}_e$ are nonzero; we denote these eigenvalues as $\lambda_0, \ldots, \lambda_{r_a(e)-1}$. At high signal-to-noise ratio (SNR), the average PEP can thus be expressed as

$$P(\boldsymbol{s}\to\boldsymbol{s}') \leq \left(\prod_{q=0}^{r_a(e)-1}\lambda_q\right)^{-1}\left(\frac{1}{4N_0}\right)^{-r_a(e)}$$

where $r_a(e)$ is the diversity gain, and $\left(\prod_{q=0}^{r_a(e)-1}\lambda_q\right)^{1/r_a(e)}$ is the coding gain for the error pattern $\boldsymbol{e} := \boldsymbol{s}-\boldsymbol{s}'$. Since $r_a(e)$ depends on $\boldsymbol{e}$, taking a conservative approach we will define *the diversity order* of our system as $G_d := \min_{\forall\,\boldsymbol{e}\neq 0} r_a(e)$. Because $\boldsymbol{A}_e$ is an $r_h\times r_h$ matrix, we also have that $r_a(e)\leq r_h, \forall\,\boldsymbol{e}\neq\boldsymbol{0}$. Thus, we have established the following result.

Proposition 1: If the correlation matrix of the BEM channel coefficients in (7) has rank r_h, then the Doppler diversity order of the time-selective BEM in (5) and (6) is $G_d \leq r_h$. When $\boldsymbol{R}_h$ has full rank $r_h = Q+1$, the maximum diversity order is $G_{d,\max} = Q+1$; i.e., the number of bases in the BEM determines the maximum diversity-based system performance.

Notice that Proposition 1 quantifies nicely the maximum Doppler diversity order for both correlated and i.i.d. time-selective channels, but says nothing on whether and how the maximum diversity order r_h is achievable. For transmissions over frequency-selective channels, [15] proved that carefully designed linear precoding implemented via a matrix $\boldsymbol{\Theta}$ having entries over the complex field enables maximum multipath diversity. We will show here that maximum Doppler diversity can be enabled with appropriate linearly precoded transmissions over time-selective channels as well.

To achieve maximum Doppler diversity order, the matrix

$$\boldsymbol{A}_e := (\boldsymbol{V}_h\boldsymbol{D}_h^{\frac{1}{2}})^{\mathcal{H}}\boldsymbol{\Phi}_e^{\mathcal{H}}\boldsymbol{\Phi}_e\boldsymbol{V}_h\boldsymbol{D}_h^{\frac{1}{2}}$$

must have full rank $Q+1\ \forall\,\boldsymbol{e}\neq\boldsymbol{0}$. If $N\geq Q+1$, the matrix $\boldsymbol{\Phi}_e$ (defined as in (6)) is tall. To guarantee that $\boldsymbol{A}_e$ has full rank $\forall\, r_h \in [1,\, Q+1]$, $\boldsymbol{\Phi}_e^{\mathcal{H}}\boldsymbol{\Phi}_e$ should have full rank. Because $\mathrm{rank}(\boldsymbol{\Phi}_e^{\mathcal{H}}\boldsymbol{\Phi}_e) = \mathrm{rank}(\boldsymbol{\Phi}_e)$, the maximum diversity is achieved if and only if $\boldsymbol{\Phi}_e$ has full rank, $\forall\,\boldsymbol{e}\neq\boldsymbol{0}$. Now let us go back to the definition of $\boldsymbol{\Phi}_e$ (c.f. (6)) to devise design criteria for $\boldsymbol{\Theta}$ that guarantee the full rank of $\boldsymbol{\Phi}_e$, $\forall\,\boldsymbol{e}\neq\boldsymbol{0}$.

Recalling that $\boldsymbol{u} := \boldsymbol{\Theta}\boldsymbol{s}$, and defining $\boldsymbol{u}_e := \boldsymbol{\Theta}\boldsymbol{e}$, we can express the matrix $\boldsymbol{\Phi}_e$ as

$$\begin{aligned}\boldsymbol{\Phi}_e &= [\boldsymbol{D}(\omega_0)\boldsymbol{u}_e, \ldots, \boldsymbol{D}(\omega_Q)\boldsymbol{u}_e]\\ &:= \mathrm{diag}[\boldsymbol{u}_e]\cdot[\boldsymbol{d}_0, \ldots, \boldsymbol{d}_Q] \qquad (8)\end{aligned}$$

where $[\boldsymbol{d}_q]_k := \exp(j\omega_q k)$, for $k\in[0,\, N-1]$, $q\in[0,\, Q]$. Because $[\boldsymbol{d}_0, \ldots, \boldsymbol{d}_Q]$ is a tall column-wise Vandermonde matrix, and the frequencies in the set $\{\omega_q := 2\pi(q-Q/2)/N\}_{q=0}^{Q}$ are all equi-spaced, by defining $\overline{\omega} := \omega_q - \omega_{q-1}, \forall\, q$, we can verify that

$$[\boldsymbol{d}_0, \ldots, \boldsymbol{d}_Q] = \boldsymbol{D}(\omega_0)[\overline{\boldsymbol{d}}_0, \ldots, \overline{\boldsymbol{d}}_Q]$$

where

$$[\overline{\boldsymbol{d}}_q]_k := \exp(j\overline{\omega}qk), \qquad k\in[0,\, N-1].$$

Notice that the matrix $[\overline{\boldsymbol{d}}_0, \ldots, \overline{\boldsymbol{d}}_Q]$ is a Vandermonde matrix with distinct generators both column-wise and row-wise; hence, *any* $Q+1$ *rows of the matrix* $[\overline{\boldsymbol{d}}_0, \ldots, \overline{\boldsymbol{d}}_Q]$ *are linearly independent*, which establishes the following proposition.

Proposition 2: For linearly precoded transmissions over a time-selective BEM obeying the input–output relationship (5), the maximum Doppler diversity gain $G_d = r_h \leq Q+1$ is enabled with a precoder $\boldsymbol{\Theta}$ if and only if there exist at least $Q+1$ nonzero entries in $\boldsymbol{u}_e = \boldsymbol{\Theta}\boldsymbol{e}$, $\forall\,\boldsymbol{e}\neq\boldsymbol{0}$.

Proof: Appendix B.

In the following, we will introduce three classes of linear precoders which satisfy the necessary and sufficient condition of Proposition 2.

Tall Vandermonde Precoders: Consider $N\geq N_s+Q$ distinct points $\{\rho_n\}_{n=1}^{N}\in\mathbb{C}$, where $\mathbb{C}$ denotes the complex field. With generators $\{\rho_n\}_{n=1}^{N}$, we construct a row-wise tall Vandermonde precoder $\boldsymbol{\Theta}\in\mathbb{C}^{N\times N_s}$ with entries $[\boldsymbol{\Theta}]_{n,k} = \rho_n^k$. Consider now a polynomial $\psi_e(x)$ of order N_s-1 with nonzero coefficients $\boldsymbol{e}$; it can be verified that $\boldsymbol{\Theta}\boldsymbol{e} = [\psi_e(\rho_1), \ldots, \psi_e(\rho_N)]^T$. Since $\psi_e(x)$ has at most N_s-1 roots, $\{\psi_e(\rho_n)\}_{n=1}^{N}$ has at most N_s-1 zero elements; i.e., at least $N-(N_s-1)\geq Q+1$ nonzero elements. Therefore, these tall Vandermonde precoders satisfy the condition of Proposition 2, and can thus achieve the maximum Doppler diversity order.

As a special case, we can choose $\boldsymbol{\Theta} = \boldsymbol{F}_N^{\mathcal{H}}\boldsymbol{T}_{zp}$, where $\boldsymbol{F}_N^{\mathcal{H}}$ is the N-point inverse FFT (IFFT) matrix, and $\boldsymbol{T}_{zp} := [\boldsymbol{I}_{N_s}\quad \boldsymbol{0}_{N_s\times Q}]^T$. Applying this precoder to each symbol block $\boldsymbol{s}$ consists of two steps: first, the information block $\boldsymbol{s}$ is padded with Q zeros (via $\boldsymbol{T}_{zp}$), and then the zero-padded block is processed by an N-point IFFT (via $\boldsymbol{F}_N^{\mathcal{H}}$).

Tall Vandermonde precoders are redundant, but guarantee maximum diversity regardless of the constellation. In contrast, our next class will be nonredundant but constellation specific.

Square Precoders: It has been proved that if the symbols in $\boldsymbol{s}$ are drawn from a quadrature amplitude modulation (QAM) (or pulse amplitude modulation (PAM)) constellation, there always exists a square Vandermonde matrix $\boldsymbol{V}$ such that $\boldsymbol{u}_e = \boldsymbol{V}\boldsymbol{e}$ has no entry equal to zero $\forall\,\boldsymbol{e}\neq\boldsymbol{0}$ [16]. Based on this property, we design our square $(N_s = N)$ precoder as

$$\boldsymbol{\Theta} = \begin{bmatrix}\boldsymbol{I}_{N_g}\otimes\boldsymbol{v}_1^T\\ \vdots\\ \boldsymbol{I}_{N_g}\otimes\boldsymbol{v}_{N_{\mathrm{sub}}}^T\end{bmatrix}_{N\times N} \qquad (9)$$

where $\boldsymbol{v}_m^T$ is the mth row of an $N_{\mathrm{sub}}\times N_{\mathrm{sub}}$ precoder $\boldsymbol{V}$, with $N = N_{\mathrm{sub}}N_g$. The design of $\boldsymbol{V}$ is detailed in [14], [16], [8] and references therein, and guarantees that $\boldsymbol{V}\boldsymbol{e}$ has no zero entry $\forall\,\boldsymbol{e}\neq\boldsymbol{0}$. So long as we select $N_{\mathrm{sub}}\geq Q+1$, the maximum diversity is enabled by the precoder in (9) [8].

As an example, for $N_{\mathrm{sub}} = 5$, the square $\boldsymbol{\Theta}$ ensures maximum Doppler diversity by designing $[\boldsymbol{V}]_{n,k} = \rho_n^k$ [14], [16], where

$$\left\{\rho_n = 2^{1/(2N_{\mathrm{sub}})}e^{j(\pi/4+2\pi n)/N_{\mathrm{sub}}}\right\}_{n=0}^{N_{\mathrm{sub}}-1}.$$

Since the time-selective channel matrix is diagonal, based on the special structure of $\boldsymbol{\Theta}$ in (9), we can break each block of size N into N_g subblocks. Note that decoding here is performed per subblock of size N_{sub}. Therefore, decoding complexity depends on the subblock size N_{sub}. Hence, the square precoder in (9) leads to lower decoding complexity than the tall Vandermonde one.

SS Precoders: For SS transmissions, each information symbol is spread by a factor N_c. In this case, the precoded block length is $N =$

N_cN_s. From Proposition 2, we know that in order to achieve full diversity, the spreading gain N_c should be greater than or equal to $Q+1$. If $\boldsymbol{\theta}$ denotes the spreading vector, the SS precoder can be written as

$$\boldsymbol{\Theta} = \begin{bmatrix} \theta_1 \boldsymbol{I}_{N_s} \\ \vdots \\ \theta_{N_c} \boldsymbol{I}_{N_s} \end{bmatrix}_{N \times N_s} \tag{10}$$

where θ_m is the mth entry of $\boldsymbol{\theta}$. Since we only consider the single-user case in this correspondence, without loss of generality, we assume $\theta_m = 1/\sqrt{N_c}$, $\forall m$. From the structure of $\boldsymbol{\Theta}$ in (10), we observe that $\boldsymbol{\Theta}$ performs not only spreading but also chip interleaving (CI). In the simulation section (see Section IV), we will demonstrate the importance of CI on performance.

When each block contains one symbol ($N_s = 1$), the precoder $\boldsymbol{\Theta}$ reduces to an $N \times 1$ vector $\boldsymbol{\theta}$. Any SS transmission with $N_c < Q+1$ cannot guarantee the maximum diversity order, even if ML decoding is employed. This result shows that for a single user, the time–frequency approach of [2], [12] can collect only the full diversity at the receiver provided that the chip period (also the sampling period) $T_c = T_s$ is chosen to ensure that $2f_{\max}T_s < 1$. Unfortunately, for point-to-point links, this class of SS precoders consumes more bandwidth relative to the first two classes.

Remark 1: For a given $f_{\max}$, as the number of symbols per block N, or the sampling period (equals symbol period) T_s, increases, Q increases as well. If the scattering is sufficiently rich to ensure that $r_h = Q+1$, then the diversity increases. However, longer block lengths result in longer decoding delays, and require higher decoding complexity. SS precoders can afford RAKE reception with lower complexity than ML (or near-ML) decoding for the first two classes of precoders. However, for single-user links, SS precoders sacrifice bandwidth efficiency.

B. Time- and Frequency-Selective Channels

In this subsection, we will design maximum diversity transmissions through doubly selective channels. Intuitively, one would expect that doubly selective channels can provide joint Doppler and multipath diversity (see also [2], [12]). However, except for bandwidth-consuming SS systems, designing the general diversity enabling precoders for doubly selective channels is challenging. In the following, we will solve this problem systematically. Plugging (4) into (3), we obtain

$$\boldsymbol{y}(n) = \sum_{q=0}^{Q} \boldsymbol{D}(\omega_q)\left[\boldsymbol{H}_q^{(0)}(n)\boldsymbol{u}(n) + \boldsymbol{H}_q^{(1)}(n)\boldsymbol{u}(n-1)\right] + \boldsymbol{w}(n) \tag{11}$$

where $\boldsymbol{u}(n) := \boldsymbol{\Theta}\boldsymbol{s}(n)$. Using the commutativity of products of Toeplitz (convolution) matrices with vectors, we find that

$$\boldsymbol{H}_q^{(0)}(n)\boldsymbol{u}(n) = \boldsymbol{U}^{(0)}(n)\boldsymbol{h}_q(n)$$

$$\boldsymbol{H}_q^{(1)}(n)\boldsymbol{u}(n-1) = \boldsymbol{U}^{(1)}(n-1)\boldsymbol{h}_q(n)$$

where

$$[\boldsymbol{h}_q(n)]_l := h_q(n;\, l), \qquad l \in [0,\, L]$$

while $\boldsymbol{U}^{(0)}(n)$ and $\boldsymbol{U}^{(1)}(n-1)$ are $N \times (L+1)$ Toeplitz matrices with first column $[u_1(n),\, \ldots,\, u_N(n)]^T$, and first row $[0,\, u_N(n-1),\, \ldots,\, u_{N-L+1}(n-1)]$, respectively. Defining

$$\boldsymbol{U}(n) := \boldsymbol{U}^{(0)}(n) + \boldsymbol{U}^{(1)}(n-1)$$

we can rewrite (11) as

$$\begin{aligned} \boldsymbol{y}(n) &= \sum_{q=0}^{Q} \boldsymbol{D}(\omega_q)\boldsymbol{U}(n)\boldsymbol{h}_q(n) + \boldsymbol{w}(n) \\ &= \boldsymbol{\Phi}_s(n)\boldsymbol{h}(n) + \boldsymbol{w}(n) \end{aligned} \tag{12}$$

where, similar to (5), we define the $N \times (Q+1)(L+1)$ matrix $\boldsymbol{\Phi}_s(n)$, and the augmented $(Q+1)(L+1) \times 1$ channel vector $\boldsymbol{h}(n)$, respectively, as

$$\boldsymbol{\Phi}_s(n) := [\boldsymbol{D}(\omega_0)\boldsymbol{U}(n),\, \ldots,\, \boldsymbol{D}(\omega_Q)\boldsymbol{U}(n)] \tag{13}$$

and

$$\boldsymbol{h}(n) := \left[\boldsymbol{h}_0^T(n),\, \ldots,\, \boldsymbol{h}_Q^T(n)\right]^T. \tag{14}$$

Noticing the similarity between (12) and (5), the augmented channel correlation matrix and its rank will be likewise defined as

$$\boldsymbol{R}_h := E[\boldsymbol{h}(n)\boldsymbol{h}^{\mathcal{H}}(n)] \quad \text{and} \quad r_h := \operatorname{rank}(\boldsymbol{R}_h) \le (Q+1)(L+1)$$

respectively. Mimicking the steps used to prove Proposition 1, we can establish the following result for time- and frequency-selective channels.

Proposition 3: If the correlation matrix of the BEM channel vector in (14) has rank r_h, then the maximum diversity order (a.k.a. multipath-Doppler diversity order) of the doubly selective channel in (12) is $G_d = r_h$. When $\boldsymbol{R}_h$ has full rank $r_h = (L+1)(Q+1)$, the maximum diversity gain is $G_{d,\max} = (L+1)(Q+1)$.

Notice that Proposition 3 specifies that the maximum possible diversity order is multiplicative in the discrete-time equivalent BEM parameters L and Q. More importantly, Proposition 3 asserts that the achievable diversity order equals the rank r_h of the BEM coefficients' correlation matrix.

In a nutshell, what determines the diversity-based performance when transmitting over a doubly selective environment is the number of the *effective degrees of freedom* that the channel possesses after sampling; and this can be described by a single BEM parameter, namely, the rank r_h of the underlying channel correlation matrix.

Generalizing the analysis of Section III-A to doubly selective channels, we deduce that in order to achieve full diversity, we need to design $\boldsymbol{\Theta}$ so that $\operatorname{rank}(\boldsymbol{\Phi}_e(n)) = (Q+1)(L+1)$, $\forall\, \boldsymbol{e}(n) \neq \boldsymbol{0}$.

To guarantee the latter, the following conditions are necessary.

C1) *The transmitted block length is chosen to satisfy*

$$N \ge (Q+1)(L+1).$$

C2) *The precoder $\boldsymbol{\Theta}$ is selected so that $\boldsymbol{U}(n)$ in* (13) *has full rank*

$$\forall\, \boldsymbol{u}(n) := \boldsymbol{\Theta}\boldsymbol{s}(n) \neq \boldsymbol{0}.$$

Being only necessary conditions, C1) and C2) do not provide us with sufficient guidelines to design precoders $\boldsymbol{\Theta}$ that guarantee full diversity. For this reason, we will synthesize first a specific precoder, and then we will generalize it to a class of precoders. Consider the $N \times N_s$ matrix

$$\boldsymbol{\Theta} = \boldsymbol{F}_{P+Q}^{\mathcal{H}}\boldsymbol{T}_1 \otimes \boldsymbol{T}_2 \tag{15}$$

where $\boldsymbol{F}_{P+Q}^{\mathcal{H}}$ is a $(P+Q)$-point IFFT matrix $\boldsymbol{T}_1 := [\boldsymbol{I}_P,\, \boldsymbol{0}_{P\times Q}]^T$, and $\boldsymbol{T}_2 = [\boldsymbol{I}_K,\, \boldsymbol{0}_{K\times L}]^T$. Notice that this IFFT-based precoder inserts zero guards in both the time (via $\boldsymbol{T}_2$) and in the frequency dimensions (via $\boldsymbol{T}_1$). Note that the precoder in (15) is the single-user counterpart of the precoders proposed in [7] that include also user-specific spreading codes $\boldsymbol{c}_u$ to enable multiple access regardless of time- and frequency-selective fading effects. In fact, (15) coincides with the precoder in [7], if $\boldsymbol{c}_u$ is replaced by 1 for the single user indexed by u.

For this precoder, we select sizes $N_s = PK$ and $N = (P+Q)(K+L)$. Condition C1) can be easily fulfilled by choosing $P \ge 1$ and $K \ge 1$. Since the trailing zeros of $\boldsymbol{T}_2$ force the last L rows of $\boldsymbol{\Theta}$ to be zero, it can be verified that $\boldsymbol{H}_q^{(1)}(n)\boldsymbol{\Theta} = \boldsymbol{0}$, $\forall\, q$. The latter implies that IBI

is eliminated from (3), and hence block-by-block receiver processing becomes possible based on

$$\boldsymbol{y}(n) = \sum_{q=0}^{Q} \boldsymbol{D}(\omega_q)\boldsymbol{H}_q^{(0)}(n)\boldsymbol{\Theta}\boldsymbol{s}(n) + \boldsymbol{w}(n). \tag{16}$$

Since $\boldsymbol{H}_q^{(0)}(n)\boldsymbol{\Theta}$ is a Toeplitz matrix with first column $[h_q(n;\,0),\,\ldots,\,h_q(n;\,L),\,0,\,\ldots,\,0]^T$, we deduce that $\boldsymbol{U}(n)$ in (13) is a Toeplitz matrix, which satisfies C2).

Until now, we have only verified that the design of $\boldsymbol{\Theta}$ in (15) satisfies C1) and C2). To prove the full diversity, we need to further show that $\boldsymbol{\Phi}_e$ (defined as in (13)) has full rank $\forall\, \boldsymbol{e} \neq \boldsymbol{0}$. For brevity, we will drop the block index n, and throughout our proof we will make repeated use of the formula for the product of Kronecker products of matrices with matching dimensions

$$(\boldsymbol{A}_1 \otimes \boldsymbol{A}_2)(\boldsymbol{B}_1 \otimes \boldsymbol{B}_2) = (\boldsymbol{A}_1\boldsymbol{B}_1) \otimes (\boldsymbol{A}_2\boldsymbol{B}_2).$$

From the structure of $\boldsymbol{H}_q^{(0)}$, we have

$$\boldsymbol{H}_q^{(0)} = \boldsymbol{I}_{P+Q} \otimes \overline{\boldsymbol{H}}_q^{(0)} + \boldsymbol{J}_{P+Q} \otimes \overline{\boldsymbol{H}}_q^{(1)} \tag{17}$$

where $\boldsymbol{J}_{P+Q}$ is a $(P+Q)\times(P+Q)$ lower triangular Toeplitz with first column $[0,\,1,\,0,\,\ldots,\,0]^T$, and the matrix $\overline{\boldsymbol{H}}_q^{(r)}$ has the same structure as $\boldsymbol{H}_q^{(r)},\ r = 0,\,1$, except that its dimensionality is $(K+L)\times(K+L)$. Using (17) and the fact that $\overline{\boldsymbol{H}}_q^{(1)}\boldsymbol{T}_2 = \boldsymbol{0}$, we obtain

$$\begin{aligned}\boldsymbol{H}_q^{(0)}\boldsymbol{\Theta} &= \left(\boldsymbol{F}_{P+Q}^{\mathcal{H}}\boldsymbol{T}_1\right) \otimes \left(\overline{\boldsymbol{H}}_q^{(0)}\boldsymbol{T}_2\right) \\ &= \left(\boldsymbol{F}_{P+Q}^{\mathcal{H}}\boldsymbol{T}_1 \otimes \boldsymbol{I}_{K+L}\right)\left(\boldsymbol{I}_P \otimes \overline{\boldsymbol{H}}_q^{(0)}\boldsymbol{T}_2\right).\end{aligned} \tag{18}$$

Let us define the $(K+L)\times K$ matrix, $\boldsymbol{H}_q := \overline{\boldsymbol{H}}_q^{(0)}\boldsymbol{T}_2$, which is Toeplitz with first column $[\boldsymbol{h}_q^T,\,0,\,\ldots,\,0]^T$. By parsing $\boldsymbol{s}$ into P subblocks $\{\boldsymbol{s}_p\}_{p=1}^P$, each of length K, we can verify that

$$(\boldsymbol{F}_{P+Q}\boldsymbol{T}_1 \otimes \boldsymbol{I}_{K+L})(\boldsymbol{I}_P \otimes \boldsymbol{H}_q)\boldsymbol{s} = \begin{bmatrix} \overline{\boldsymbol{S}}_1 \\ \vdots \\ \overline{\boldsymbol{S}}_{P+Q} \end{bmatrix} \boldsymbol{h}_q \tag{19}$$

where

$$\overline{\boldsymbol{S}}_q := \sum_{p=1}^{P} \boldsymbol{S}_p \exp\left(j\frac{2\pi}{P+Q}(p-1)(q-1)\right), \quad \text{for } q \in [1,\,P+Q]$$

and $\{\boldsymbol{S}_p\}_{p=1}^P$ are $(K+L)\times(L+1)$ Toeplitz matrices with first column $[\boldsymbol{s}_p^T\,\boldsymbol{0}_{1\times L}]^T$. Plugging (19) into (16), and splitting $\boldsymbol{D}(\omega_q)$ into $P+Q$ submatrices of equal size, we arrive at

$$\boldsymbol{y} = \sum_{q=0}^{Q} \begin{bmatrix} \boldsymbol{D}_{q,\,1} & & \\ & \ddots & \\ & & \boldsymbol{D}_{q,\,P+Q} \end{bmatrix} \begin{bmatrix} \overline{\boldsymbol{S}}_1 \\ \vdots \\ \overline{\boldsymbol{S}}_{P+Q} \end{bmatrix} \boldsymbol{h}_q + \boldsymbol{w}$$

where $\{\boldsymbol{D}_{q,\,p}\}_{p=1}^{P+Q}$ are $(K+L)\times(K+L)$ matrices. Rewriting $\boldsymbol{\Phi}_s$ defined in (13) as

$$\boldsymbol{\Phi}_s = \begin{bmatrix} \boldsymbol{D}_{0,\,1}\overline{\boldsymbol{S}}_1 & \boldsymbol{D}_{1,\,1}\overline{\boldsymbol{S}}_1 & \cdots & \boldsymbol{D}_{Q,\,1}\overline{\boldsymbol{S}}_1 \\ \vdots & \vdots & \vdots & \\ \boldsymbol{D}_{0,\,P+Q}\overline{\boldsymbol{S}}_{P+Q} & \boldsymbol{D}_{1,\,P+Q}\overline{\boldsymbol{S}}_{P+Q} & \cdots & \boldsymbol{D}_{Q,\,P+Q}\overline{\boldsymbol{S}}_{P+Q} \end{bmatrix} \tag{20}$$

we can compactify the input–output relationship of our BEM-based doubly selective channel as $\boldsymbol{y} = \boldsymbol{\Phi}_s\boldsymbol{h} + \boldsymbol{w}$ (c.f. (12)).

Similar to Section III-A, in order to prove that the maximum diversity order is guaranteed irrespective of the underlying signal constellation, and regardless of the doubly selective channel encountered, we have to prove that $\boldsymbol{\Phi}_e$ (defined as in (20)) has full rank $(Q+1)(L+1)$ $\forall\, \boldsymbol{e} \neq \boldsymbol{0}$. We prove this fact in Appendix A, and thus establish that the precoder $\boldsymbol{\Theta} = \boldsymbol{F}_{P+Q}^{\mathcal{H}}\boldsymbol{T}_1 \otimes \boldsymbol{T}_2$ enables multiplicative Doppler-multipath diversity.

We are now ready to generalize (15) to precoders $\boldsymbol{\Theta} = \boldsymbol{V} \otimes \boldsymbol{T}_{zp}$, where $\boldsymbol{V}\boldsymbol{e}$ has at least $Q+1$ nonzero entries $\forall\, \boldsymbol{e} \neq \boldsymbol{0}$, and $\boldsymbol{T}_{zp} = [\boldsymbol{I}_K\,\boldsymbol{0}_{K\times L}]^T$. In summary, we have the following.

Proposition 4: The achievable multipath-Doppler diversity order $G_d = r_h$ is enabled by block transmissions linearly precoded with $\boldsymbol{\Theta} = \boldsymbol{V} \otimes \boldsymbol{T}_{zp}$, where $\boldsymbol{T}_{zp} = [\boldsymbol{I}_K,\,\boldsymbol{0}_{K\times L}]^T$, and $\boldsymbol{V}$ is such that $\boldsymbol{V}\boldsymbol{e}$ has at least $Q+1$ nonzero entries for any nonzero $P\times 1$ error vector $\boldsymbol{e}$. When the channel correlation matrix has full rank $r_h = (Q+1)(L+1)$, this precoder $\boldsymbol{\Theta}$ enables the maximum possible diversity gain $G_{d,\,\max} = (Q+1)(L+1)$.

It is clear that one has many choices for $\boldsymbol{V}$ to satisfy the condition of Proposition 4. An immediate choice is to select $\boldsymbol{V}$ as a tall $(P+Q)\times P$ Vandermonde matrix, or as the $P\times P$ square Vandermonde matrix. Another choice is an SS precoder, where $\boldsymbol{V}$ reduces to a $P\times 1$ vector $\boldsymbol{v}$. To guarantee the full diversity, $\boldsymbol{v}$ must have at least $Q+1$ nonzero entries.

The time–frequency RAKE receiver [2], [12] is tailored to SS transmissions. Compared with [12], our approach enables full diversity by designing not only the receiver, but also the transmitter. It enables transmit-and-receive diversity for any block transmission system, whereas [12] focuses only on SS transmissions. Precoder design for doubly selective channels was also studied in [10]; however, i) the precoders $\boldsymbol{\Theta}$ in [10] are limited to orthogonal SS codes; ii) the channel model is not as general as the BEM; and iii) the diversity order is not quantified.

Remark 2: To complete our transceiver design, we discuss briefly the decoding algorithms that are available for linearly precoded transmissions. Based on (5) and (16), we infer that linear zero-forcing (ZF) and minimum mean-square error (MMSE) decoders are applicable (see [15] and references therein for details). It is well known that such linear equalizers offer low complexity. However, they are unable to collect the full diversity. ML decoding requires an exhaustive search over the finite alphabet set $\mathcal{A}$, which has high complexity (exponential in the block length N and $\log_2|\mathcal{A}|$). A relatively less complex near-ML search is provided by the sphere-decoding (SD) algorithm [14]. A performance–complexity compromise is offered by block decision feedback equalization (B-DFE) [11]. We will resort to simulations to test the performance of these decoders.

The RAKE receiver of [2], [12] is ML optimal if only one information symbol is transmitted per block; i.e., when SS transmission is employed. Otherwise, the presence of correlation among symbols renders the RAKE suboptimum [9].

Remark 3: At least for high SNR, the overall system performance improves, as the achievable diversity increases. So far, we derived designs capable of achieving full diversity. We also recognized that increasingly higher diversity, comes at the price of higher complexity. Hence, a natural question is whether it is always necessary to achieve full diversity. Diversity orders beyond 5 show up for SNR values that are too high; hence, we would advocate BEMs with $Q \in [0,\,4]$, which imply relatively small block sizes N, and lead to affordable decoding delays. One could argue that the smallest possible Q (e.g., $Q = 0,\,2$) is always desirable, since even with moderate delay spreads (say, $L = 2$), the diversity order could be high enough $(G_d = (Q+1)(L+1) = 3,\,9)$ for practical SNR values. However, having $G_d > 6$ may have merits in rendering the performance with a lower complexity (e.g., least MMSE (LMMSE)) decoder, comparable to that of a system with $G_d \leq 6$ relying on a higher complexity (e.g., ML or sphere) decoder. In a nutshell, selecting the number of BEM bases depends on the application-specific performance vs. complexity vs. decoding delay tradeoffs.

C. Bandwidth Efficiency

We have seen that as the block length N increases, the number of bases Q increases. As Q and/or L increase, the potential diversity order also increases. However, in this case, the number of guard (redundant)

symbols also increases. In this subsection, we will study bandwidth efficiency issues pertaining to our maximum diversity transmissions with different precoders.

Consider the precoder $\boldsymbol{\Theta} = \boldsymbol{V} \otimes \boldsymbol{T}_{zp}$. For tall precoders ($\boldsymbol{V}$ is a tall matrix with size $(P+Q) \times P$), we obtain that for every $N_s = PK$ information-bearing symbols the precoder $\boldsymbol{\Theta}$ outputs $N = (P+Q)(K+L)$ symbols. Hence, the bandwidth efficiency of our transmissions is

$$\eta^{\text{tall}} := \frac{PK}{N} = \frac{K}{K+L} = K\,\frac{Q}{N}. \tag{21}$$

By tuning the parameters $(K,\ L,\ P,\ Q)$, we can adjust the bandwidth efficiency. However, these parameters are not completely independent of each other.

Given T_s, $f_{\max}$ and $\tau_{\max}$, the parameters L and Q/N are fixed. Treating K as a continuous variable, and differentiating η^{tall} with respect to K, we find that

$$\frac{\partial \eta^{\text{tall}}}{\partial K} = \frac{L}{(K+L)^2} - \frac{Q}{N} = 0$$

which yields the optimal choice of K as

$$K_{\text{opt}} = \left\lceil \sqrt{\frac{L}{Q/N}} - L \right\rfloor.$$

Since L and Q/N are fixed, we deduce that K_{opt} increases as Q increases. As N is large and $\tau_{\max} \gg T_s$, we have $L \approx \tau_{\max}/T_s$, and $Q/N \approx 2f_{\max}T_s$, which imply that

$$K_{\text{opt}} \approx \left(\sqrt{\tau_{\max}/(2f_{\max})} - \tau_{\max}\right)\Big/ T_s. \tag{22}$$

Plugging (22) into (21), we obtain the optimal η^{tall} expressed in terms of the delay-Doppler spread factor as:

$$\eta^{\text{tall}}_{\text{opt}} = \left(1 - \sqrt{2f_{\max}\tau_{\max}}\right)^2. \tag{23}$$

This result coincides with the one in [7].

Similar to tall precoders, we can obtain the bandwidth efficiency for square precoders ($\boldsymbol{V}$ is square with size $P \times P$) as

$$\eta^{\text{sq}} = \frac{K}{K+L} = 1 - \frac{PL}{N}.$$

To guarantee full diversity, we need to choose $P \geq Q+1$. In this case, the optimum bandwidth efficiency is achieved when $P = Q+1$ as

$$\eta^{\text{sq}}_{\text{opt}} = 1 - 2f_{\max}\tau_{\max}. \tag{24}$$

When $\boldsymbol{V}$ is a $P \times 1$ vector, the bandwidth efficiency is

$$\eta^{\text{ss}} = \frac{K}{P(K+L)} = \frac{1}{P} - \frac{L}{N}.$$

Similar to the square case, we find that the optimum η is obtained when $P = Q+1$ as

$$\eta^{\text{ss}}_{\text{opt}} = \frac{1 - 2f_{\max}\tau_{\max}}{2f_{\max}T_sN}. \tag{25}$$

Comparing bandwidth efficiency for these three cases (23), (24), and (25), it follows readily that

$$\eta^{\text{sq}}_{\text{opt}} > \eta^{\text{tall}}_{\text{opt}} > \eta^{\text{ss}}_{\text{opt}}. \tag{26}$$

Observing (23), (24) and (25), we notice that for underspread channels $(2f_{\max}\tau_{\max} < 1)$, the values of η_{opt}'s are all positive; hence, maximum diversity transmissions are only possible for underspread channels, which also justifies the need for assumption A1).

IV. Simulated Performance

We now present simulations to test the BEM fitting to doubly selective channels, and also confirm the performance of our maximum diversity transmissions. All the test cases will employ quaternary phase-shift keying (QPSK) modulation, and perfect channel knowledge will be assumed at the receiver. The SNR is defined as bit energy over noise power (E_b/N_0).

Test Case 1 (BEM Justification): For TV channels, the Jakes' model is widely adopted. Here, we will test how accurately the BEM can approximate it. We consider a system with carrier frequency $f_o =$ 900 MHz, and symbol duration (also sampling period) $T_s = 0.5$ ms. With maximum mobile velocity $v_{\max} = 96$ km/h, the maximum Doppler shift is $f_{\max} = 80$ Hz. We select $N = 50$. The Jakes' model is generated according to [5, p. 68]. Fig. 2 depicts one realization of the Jakes' model, along with BEM approximants corresponding to various Q values. The BEM coefficients are estimated using the least-squares algorithm of [7]. For the given triplet ($f_{\max}$, T_s, and N), we find $Q = 2\lceil f_{\max}NT_s \rceil = 4$. From Fig. 2, we verify that the larger number of bases Q we use, the better approximation we obtain. However, when $Q > 4$, there is no significant improvement in the approximation. We plot the absolute value of Fourier transform of $c(t;\,\tau)$ in Fig. 3, where

$$C(f;\,\tau) = \int_0^{NT_s} c(t;\,\tau)e^{-j2\pi tf}\,dt.$$

We also mark $f_{\max}$ and $1/NT_s$ on the same figure to illustrate that the channel is practically band limited. This allows one to sample $C(f;\,\tau)$ in the frequency domain, and ensures reliable approximation with a sufficient (but finite) number of bases. In Fig. 4, we depict the average mean-square error (MSE) between Jakes' model and BEM as a function of Q. Note that the x-axis in Fig. 4 is $Q/2$ because we defined $Q := 2\lceil f_{\max}NT_s \rceil$. We observe that: i) as the number of bases increases, the MSE goes to zero; and ii) the MSE decreases slower for $Q > 4$.

Test Case 2 (TV Frequency-Flat Channels): In this test case, we will use several examples to corroborate our claims on time-selective channels. With the Jakes' model of Test Case 1, we here choose $N =$

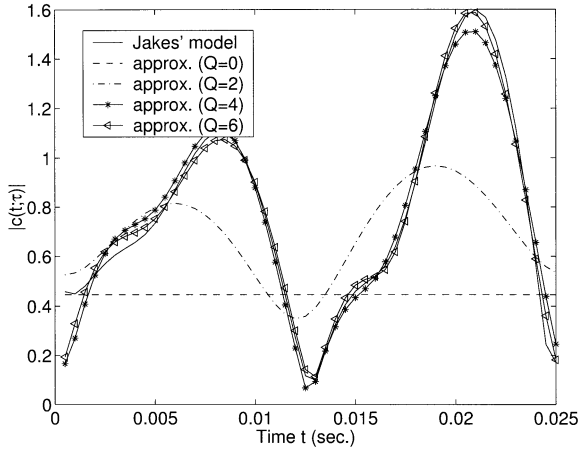

Fig. 2. Fitting Jakes' model with BEM.

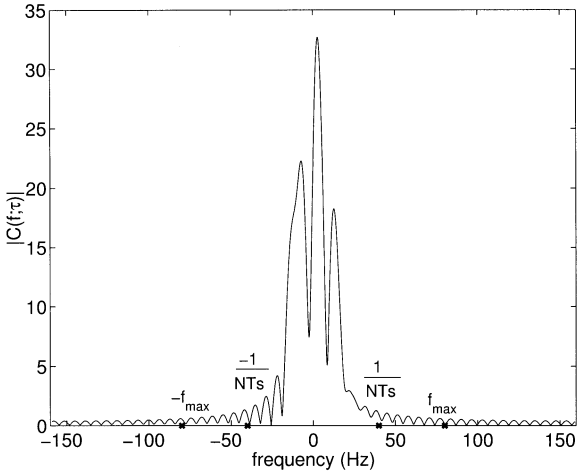

Fig. 3. Channel spectrum.

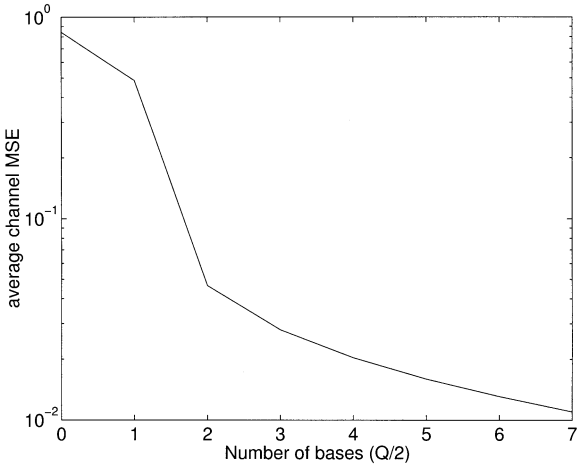

Fig. 4. Channel MSE versus the number of BEM bases.

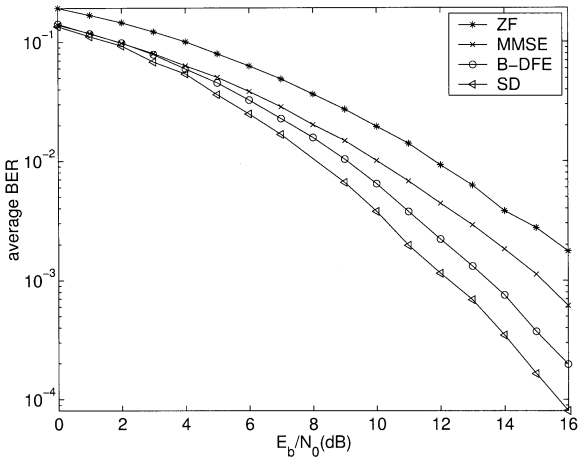

Fig. 5. Performance with different equalizers/decoders (time selective).

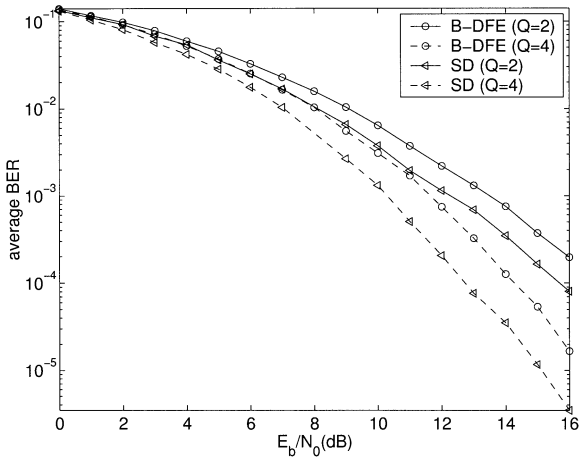

Fig. 6. Performance with precoded transmissions (time selective).

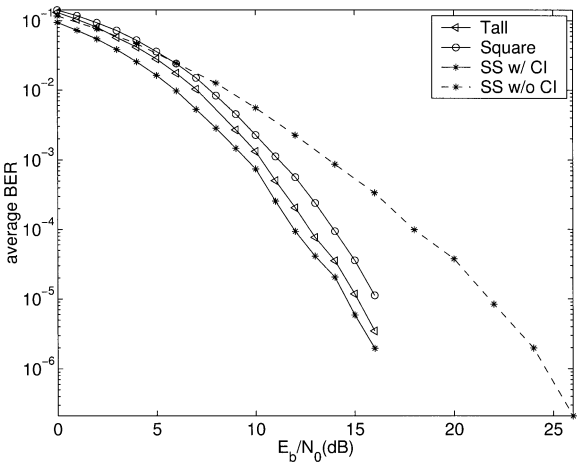

Fig. 7. Performance with various precoders (time selective).

20 and according to the choice of Q, we adjust the symbol (sampling) period as $T_s = Q/(2f_{\max}N)$.

Decoding options: For the tall Vandermonde precoder, we select $T_s = 0.625$ ms, which yields $Q = 2$. The number of information symbols is thus $N_s = N - Q = 18$. We observe from Fig. 5 that the linear MMSE outperforms the ZF equalizer by about 2 dB. B-DFE achieves diversity similar to the SD algorithm. Note that B-DFE provides a reasonable complexity–performance compromise.

Diversity orders: Here, we fix all other parameters, employ the tall precoders, and increase T_s to 1.25 ms. The BEM now entails $Q = 4$ bases. We plot the performance with SD and B-DFE in Fig. 6. Note that as Q increases (with T_s increasing), the diversity order increases as well. Observing the bit-error rate (BER) slopes in Fig. 6, we notice that SD and B-DFE achieve almost the full diversity.

Precoder options: In Section III-A, we proposed three classes of precoders. Fig. 7 compares their performance when $Q = 4$. The tall precoder is selected as the truncated FFT matrix. The square precoder is designed as in (9) with $(N_g,\ N_{\rm sub}) = (4,\ 5)$. The SS precoder with CI is designed as in (10) with $N_c = 5$. The "SS without CI" means that we simply stack the spread symbols as in [2], [12] without bit interleaving. SD is used for "tall" and "square" cases. RAKE reception is used for "SS" with or without CI. We deduce from Fig. 7 that all precoders enable the maximum diversity order (here $Q + 1 = 5$). However, they exhibit different performance because of different coding gains. The SS precoder without CI exhibits the worst performance. Note that different precoders have different bandwidth efficiency, and complexity requirements. Specifically, the SD for tall precoders has the highest decoding complexity, while the SS precoders have the lowest. The square precoder enables bandwidth efficiency $\eta = 1$, while the tall one has $\eta = 0.8$, and the SS schemes have $\eta = 0.2$. In this case, square precoders provide the desirable compromise among performance, complexity, and rate.

Variable spreading gains: We adopt the SS precoders of (10) with different spreading gains, in order to illustrate the relationship between N_c and the achieved diversity order G_d. We select $N = 60$, and chip period (equal to sampling period) $T_s = 0.417$ ms, leading to $Q = 4$. The number of symbols is $N_s = N/N_c$, and the bandwidth efficiency is $1/N_c$. Fig. 8 depicts the performance for different spreading gains. We observe that when $N_c \leq 5$, as N_c increases, the diversity increases and at the same time, the bandwidth efficiency decreases. Actually, one can prove that the achieved diversity is N_c when $N_c \leq Q+1$. However, when $N_c > 5$, as N_c increases, there is no performance gain, while the decoding complexity increases, and bandwidth efficiency decreases accordingly.

Test Case 3 (Time- and Frequency-Selective Channels): The main purpose of this example is to test our claims of Section III-B for the multiplicative diversity provided by doubly selective channels. The system parameters for our time–frequency linear precoder in (15) are $(P,\ K) = (4,\ 4)$. The $L + 1$ channel taps are independent Gaussian random with multipath power intensity profile

$$\phi_c(\tau) = \exp(-0.1\tau/T_s).$$

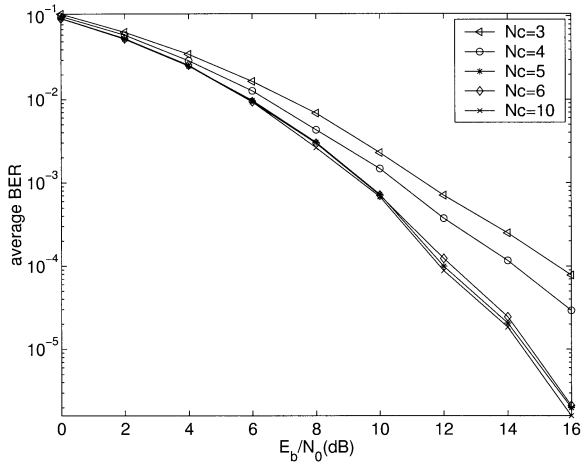

Fig. 8. Performance with variable precoder sizes (time selective).

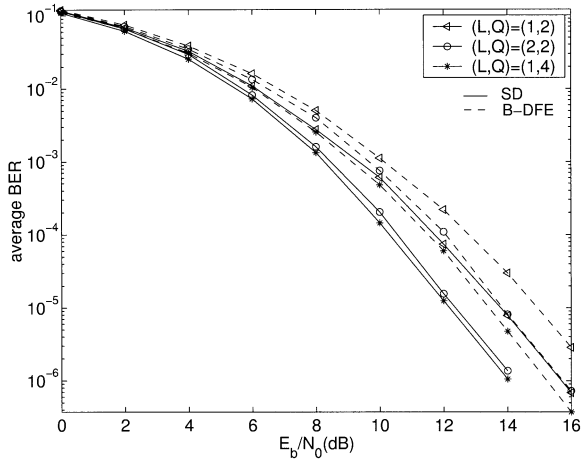

Fig. 9. Performance with precoded transmissions (doubly selective).

Each channel tap is generated by the Jakes' model using the parameters of Test Case 1. We select $N = (P+Q)(K+L)$ for desired L and Q, and then we choose T_s. SD or B-DFE is used at the receiver. Fig. 9 shows that the diversity increases as L and/or Q increase. There is less than 2-dB performance difference between the B-DFE and the SD algorithm. Observing the slope of the diversity curve when $(L, Q) = (1, 2)$, we deduce that the diversity order is $(L+1)(Q+1) = 6$. However, diversity orders 9 and 10 do not show up for the other two cases until 16 dB, which corroborates our discussion in Remark 3.

V. Conclusion

Based on a basis-expansion model (BEM) for TV channels, we proved that the maximum diversity order of time-selective channels depends on the number of bases. We designed linearly precoded transmissions that maximize the available Doppler diversity order. We also analyzed diversity transmissions through doubly selective channels. The linearly precoded and efficiently implementable transmissions that we designed enable the maximum achievable Doppler-multipath diversity order, which turned out to be the rank of the underlying channel correlation matrix. Our simulations verified our analytical claims with BEM and Jakes' channel models.

Appendix A
Proof of Full Rank for (20)

In this proof, we view $\boldsymbol{s}$ as the error vector $\boldsymbol{e}$. For every $\boldsymbol{s} \neq \boldsymbol{0}$, we know that there exists a $P \times 1$ subvector $\boldsymbol{s}'_p \neq \boldsymbol{0}$ such that

$$\boldsymbol{s}'_p := [s_p,\, s_{K+p},\, \ldots,\, s_{K(P-1)+p}]^T, \qquad \text{for } p \in [0,\, P-1].$$

One can verify that $\boldsymbol{F}^{\mathcal{H}}_{P+Q}\boldsymbol{T}_1\boldsymbol{s}'_p$ has at most $P-1$ zero entries. This implies that there are at least $Q+1$ nonzero entries in $\boldsymbol{F}^{\mathcal{H}}_{P+Q}\boldsymbol{T}_1\boldsymbol{s}'_p$. Correspondingly, the RHS of (19) has at least $Q+1$ subblocks that have full rank $L+1$. Suppose that the first $Q+1$ full rank subblocks are indexed by $n_0, \ldots, n_Q \in [1,\, P+Q]$, and define

$$\overline{\boldsymbol{\Phi}}_s := \begin{bmatrix} \boldsymbol{D}_{0,n_0}\overline{\boldsymbol{S}}_{n_0} & \boldsymbol{D}_{1,n_0}\overline{\boldsymbol{S}}_{n_0} & \cdots & \boldsymbol{D}_{Q,n_0}\overline{\boldsymbol{S}}_{n_0} \\ \vdots & \vdots & \vdots & \\ \boldsymbol{D}_{0,n_Q}\overline{\boldsymbol{S}}_{n_Q} & \boldsymbol{D}_{1,n_Q}\overline{\boldsymbol{S}}_{n_Q} & \cdots & \boldsymbol{D}_{Q,n_Q}\overline{\boldsymbol{S}}_{n_Q} \end{bmatrix}. \tag{27}$$

Since $\overline{\boldsymbol{S}}_{n_p}$ is a full-rank Toeplitz matrix, there exists a lower triangular matrix $\boldsymbol{T}_p$ formed by $L+1$ rows of $\overline{\boldsymbol{S}}_{n_p}$, starting from the first nonzero entry of $\boldsymbol{s}'_{n_p}$. This way, we can construct a $(Q+1)(L+1) \times (Q+1)(L+1)$ matrix, reducing (27) to

$$\tilde{\boldsymbol{\Phi}} = \begin{bmatrix} \tilde{\boldsymbol{D}}_{0,n_0}\boldsymbol{T}_0 & \tilde{\boldsymbol{D}}_{1,n_0}\boldsymbol{T}_0 & \cdots & \tilde{\boldsymbol{D}}_{Q,n_0}\boldsymbol{T}_0 \\ \vdots & \vdots & \cdots & \vdots \\ \tilde{\boldsymbol{D}}_{0,n_Q}\boldsymbol{T}_Q & \tilde{\boldsymbol{D}}_{1,n_Q}\boldsymbol{T}_Q & \cdots & \tilde{\boldsymbol{D}}_{Q,n_Q}\boldsymbol{T}_Q \end{bmatrix}$$

where the diagonal matrix $\tilde{\boldsymbol{D}}_{q,n_p}$ is formed by the first $L+1$ rows and columns of $\boldsymbol{D}_{q,n_p}$. Let us now define the $(Q+1)(L+1) \times 1$ vector $\boldsymbol{c}_{l,q}$ as the lth column in the qth subblock of $\tilde{\boldsymbol{\Phi}}$. To prove the full rank of $\tilde{\boldsymbol{\Phi}}$, we only need to prove that $\alpha_{l,q} = 0, \forall l,\, q$, if

$$\sum_{l=0}^{L}\sum_{q=0}^{Q}\alpha_{l,q}\boldsymbol{c}_{l,q} = \boldsymbol{0}. \tag{28}$$

Considering the $p(L+1)$th equation in (28), and taking into account the diagonal structure of $\boldsymbol{T}_p$, we obtain that

$$\begin{bmatrix} e^{j\omega_0\overline{n}_0}T_0(0) & e^{j\omega_1\overline{n}_0}T_0(0) & \cdots & e^{j\omega_Q\overline{n}_0}T_0(0) \\ \vdots & \vdots & \cdots & \vdots \\ e^{j\omega_0\overline{n}_Q}T_Q(0) & e^{j\omega_1\overline{n}_Q}T_Q(0) & \cdots & e^{j\omega_Q\overline{n}_Q}T_Q(0) \end{bmatrix}\begin{bmatrix} \alpha_{0,0} \\ \vdots \\ \alpha_{0,Q} \end{bmatrix} = \boldsymbol{0}_{(Q+1)\times 1} \tag{29}$$

where $T_p(0)$ denotes the first element of the diagonal of $\boldsymbol{T}_p$, and $\overline{n}_p = n_p(K+L)$. It is easy to verify that the first matrix on the left—hand side (LHS) of (29) has full rank. This implies that $\alpha_{0,q} = 0, \forall q$, and allows us to simplify (28) as $\sum_{l=1}^{L}\sum_{q=0}^{Q}\alpha_{l,q}\boldsymbol{c}_{l,q} = \boldsymbol{0}$. Similarly, we can find $Q+1$ equations for $\alpha_{1,q}$'s, and prove that $\alpha_{1,q} = 0$, $\forall q$. Finally, we can verify that $\alpha_{l,q} = 0, \forall l,\, q$, so that $\tilde{\boldsymbol{\Phi}}$ has rank $(Q+1)(L+1)$. Therefore, $\overline{\boldsymbol{\Phi}}_s$ in (27) has full rank $(Q+1)(L+1)$, and so does $\boldsymbol{\Phi}_s, \forall \boldsymbol{s} \neq \boldsymbol{0}$. □

Appendix B
Proof of Proposition 2

Suppose $\boldsymbol{u}_e = \boldsymbol{\Theta}\boldsymbol{e}, \forall \boldsymbol{e} \neq \boldsymbol{0}$ has at least $Q+1$ nonzero entries. Then, without loss of generality, we let the first $Q+1$ nonzero entries of $\boldsymbol{u}_e$ be $\overline{\boldsymbol{u}} = [u_{n_0}, \ldots, u_{n_Q}]^T$, where $n_q \in [0,\, N-1]$, and u_{n_q} denotes the n_qth entry of $\boldsymbol{u}_e$. Selecting the corresponding rows $\{n_q\}_{q=0}^{Q}$ of the matrix $[\boldsymbol{d}_0, \ldots, \boldsymbol{d}_Q]$, we obtain a $(Q+1) \times (Q+1)$ matrix $\boldsymbol{D}(\overline{\boldsymbol{u}})\overline{\boldsymbol{D}}(\omega_0)\boldsymbol{V}_1$, where the $(Q+1) \times (Q+1)$ Vandermonde matrix

$\boldsymbol{V}_1$ is formed by the corresponding $Q+1$ rows of $[\boldsymbol{d}^0, \ldots, \boldsymbol{d}^Q]$, and $\overline{\boldsymbol{D}}(\omega_0)$ is a diagonal matrix with those selected $Q+1$ entries from $\boldsymbol{D}(\omega_0)$ on its main diagonal. Since $\mathrm{rank}(\boldsymbol{D}(\overline{\boldsymbol{u}})\overline{\boldsymbol{D}}(\omega_0)) = Q+1$ and $\mathrm{rank}(\boldsymbol{V}_1) = Q+1$, we deduce that $\mathrm{rank}(\boldsymbol{\Phi}_e) = Q+1, \forall \boldsymbol{e} \neq \boldsymbol{0}$.

Next, we prove the "only if" part by contradiction. Suppose that for some $\boldsymbol{e}$, $\boldsymbol{u} = \boldsymbol{\Theta e}$ has only $\overline{Q}+1 < Q+1$ nonzero corresponding entries, that we collect in $\overline{\boldsymbol{u}} = [u_{n_0}, \ldots, u_{n_{\overline{Q}}}]^T$. Then, similarly to the "if" part, we can group the nonzero rows in a matrix $\boldsymbol{D}(\overline{\boldsymbol{u}})\overline{\boldsymbol{D}}(\omega_0)\boldsymbol{V}_1$. Now this $\boldsymbol{V}_1$ is a $(\overline{Q}+1)\times(Q+1)$ matrix, while $\overline{\boldsymbol{D}}(\omega_0)$ is a $(\overline{Q}+1)\times(\overline{Q}+1)$ matrix. It follows immediately that

$$\mathrm{rank}(\boldsymbol{V}_1) = \overline{Q}+1 < Q+1$$

and, hence, $\mathrm{rank}(\boldsymbol{\Phi}_e) < Q+1$, which implies that the maximum diversity cannot be achieved. □

REFERENCES

[1] P. A. Bello, "Characterization of randomly time-variant linear channels," *IEEE Trans. Commun. Syst.*, vol. CS-11, pp. 360–393, Dec. 1963.

[2] S. Bhashyam, A. M. Sayeed, and B. Aazhang, "Time-selective signaling and reception for communication over multipath fading channels," *IEEE Trans. Commun.*, vol. 48, pp. 83–94, Jan. 2000.

[3] E. Biglieri, J. Proakis, and S. Shamai (Shitz), "Fading channels: Information-theoretic and communications aspects," *IEEE Trans. Inform. Theory*, vol. 44, pp. 2619–2692, Oct. 1998.

[4] G. B. Giannakis and C. Tepedelenlioğlu, "Basis expansion models and diversity techniques for blind identification and equalization of time-varying channels," *Proc. IEEE*, vol. 86, pp. 1969–1986, Nov. 1998.

[5] W. C. Jakes, *Microwave Mobile Communications*. New York: Wiley, 1974.

[6] T. Kailath, "Measurements on time-variant communication channels," *IEEE Trans. Inform. Theory*, vol. IT-8, pp. S229–S236, Sept. 1962.

[7] G. Leus, S. Zhou, and G. B. Giannakis, "Multi-user spreading codes retaining orthogonality through unknown time- and frequency-selective fading," in *Proc. GLOBECOM Conf.*, vol. 1, San Antonio, TX, Nov. 25–29, 2001, pp. 259–263.

[8] X. Ma and G. B. Giannakis, "Complex field coded MIMO systems: Performance, rate, and tradeoffs," *Wireless Commun. Mobile Comput.*, pp. 693–717, Nov. 2002.

[9] J. G. Proakis, *Digital Communications*, 4th ed. New York: McGraw-Hill, 2001.

[10] M. Reinhardt, J. Egle, and J. Lindner, "Transformation methods, coding and equalization for time- and frequency-selective channels," *Europ. Trans. Telecommun.*, vol. 11, no. 6, pp. 555–565, Nov./Dec. 2000.

[11] A. Stamoulis, G. B. Giannakis, and A. Scaglione, "Block FIR decision-feedback equalizers for filterbank precoded transmissions with blind channel estimation capabilities," *IEEE Trans. Commun.*, vol. 49, pp. 69–83, Jan. 2001.

[12] A. M. Sayeed and B. Aazhang, "Joint multipath-doppler diversity in mobile wireless communications," *IEEE Trans. Commun.*, vol. 47, pp. 123–132, Jan. 1999.

[13] M. K. Tsatsanis and G. B. Giannakis, "Equalization of rapidly fading channels: Self-recovering methods," *IEEE Trans. Commun.*, vol. 44, pp. 619–630, May 1996.

[14] E. Viterbo and J. Boutros, "A universal lattice code decoder for fading channels," *IEEE Trans. Inform. Theory*, vol. 45, pp. 1639–1642, July 1999.

[15] Z. Wang and G. B. Giannakis, "Linearly precoded or coded OFDM for wireless channels?," in *Proc. 3rd Workshop Signal Processing Advances in Wireless Communications*, Taiwan, ROC, Mar. 20–23, 2001, pp. 267–269.

[16] Y. Xin, Z. Wang, and G. B. Giannakis, "Space-time constellation-rotating codes maximizing diversity and coding gains," *IEEE Trans. Wireless Commun.*, vol. 2, pp. 294–309, Mar. 25–27, 2003.

On Continuous-Time Optimal Deterministic Traffic Regulation

Chia-Sheng Chang, *Member, IEEE,* and
Kwang-Cheng Chen, *Senior Member, IEEE*

***Abstract*—In this correspondence, we study the continuous-time deterministic traffic regulation problem. We propose a regulation form shown to be the optimal deterministic traffic regulator in the sense that it outputs the most packets while satisfying the constraint on the output process. We further investigate the subtle relation between continuous-time and discrete-time optimal deterministic regulators, and reduce our general regulation form to the known discrete-time optimal deterministic regulator when restricting arrival (departure) instants to integers and packet size to unity. Therefore, by extending traffic-regulation theory to continuous time, our work provides a fundamental framework for future research regarding quality-of-service (QoS)-guaranteed network design/analysis in continuous-time.**

***Index Terms*—Constrained optimization, network flows, quality-of-service (QoS), traffic management.**

I. INTRODUCTION

Traffic regulation has been widely accepted as an indispensable technique to provide quality-of-service (QoS)-guaranteed multimedia services in packet-switching communication networks (e.g., TCP/IP networks [1], asynchronous transfer mode (ATM) [2]). According to [3], a traffic source conforms to a nondecreasing, nonnegative function f if $R[t-\tau, t) \leq f(\tau)$ for *all* $\tau, t \geq 0$, where $R[t-\tau, t)$ (bits) denotes the amount of information bits in packets arriving in time interval $[t-\tau, t)$. A deterministic traffic regulator with constraint function f is a filter shaping an arbitrary traffic input such that the output process conforms to f.

For *discrete-time* systems, Chang [4] studied discrete-time deterministic traffic regulators in great detail and developed a general filtering method for traffic regulation. For *continuous-time* traffic regulation, a number of results also have been proposed in the literature. A special traffic regulator called leaky bucket (σ, ρ) regulator was discussed in [5]–[8]. The $(\vec{\sigma}, \vec{\rho})$ regulators were investigated in [3], [9], [10]. However, regulators of the $(\vec{\sigma}, \vec{\rho})$ type are limited to those with concave constraint functions. In [11], regulators with *nonconcave* constraint functions can be realized with a cascade of leaky buckets with *state-dependent* token generation rates, but the detailed implementation was left unspecified. In [12] and [13], Le Boudec successfully applied the continuous-time "network calculus" [14], [4], [15], [16] to traffic shapers, and we can further improve Le Boudec's results in several aspects. First, the regulators Le Boudec considered are *bit-processing* devices which assume *fluid* input streams. In practical packet-switching networks, data arrivals are packets or cells, and thus this assumption is generally not true. Second, the *continuity property* of constraint functions is very important to the derivation of the optimal regulation formulas, but this issue

Manuscript received July 15, 2001; revised November 11, 2002. This work was supported by the Ministry of Education, Taiwan, ROC, under Contract 89E-FA06-2-4-7.

C.-S. Chang is with Delta Networks, Inc., Taipei, Taiwan, ROC (e-mail: changchias@ieee.org).

K.-C. Chen is with the Institute of Communications Engineering and Department of Electrical Engineering, National Taiwan University, Taipei, Taiwan, ROC (e-mail: chenkc@cc.ee.ntu.edu.tw).

Communicated by V. Anantharam, Associate Editor for Communication Networks.

Digital Object Identifier 10.1109/TIT.2003.813489